UC Irvine

UC Irvine Electronic Theses and Dissertations

Title

Measuring Biomechanical Properties of Cancer Cells Using a High-Throughput Microfluidic Platform and Their Correlation with Surface Rheology and Internal Elasticity

Permalink

https://escholarship.org/uc/item/74n064v2

Author

Mousapour, Bahar

Publication Date

2016

Peer reviewed|Thesis/dissertation

eScholarship.org Powered by the California Digital Library
University of California

UNIVERSITY OF CALIFORNIA,
IRVINE

Measuring Biomechanical Properties of Cancer Cells Using a High-Throughput Microfluidic Platform and Their Correlation with Surface Rheology and Internal Elasticity

THESIS

submitted in partial satisfaction of the requirements
for the degree of

MASTER OF SCIENCE

in Biomedical Engineering

by

Bahar Mousapour

Thesis Committee:
Assistant Professor Jered Haun, Chair
Professor William Tang
Associate Professor Weian Zhao

2016

© 2016 Bahar Mousapour

DEDICATION

To

my parents for their unconditional support

TABLE OF CONTENTS

LIST OF FIGURES

LIST OF TABLES

ACKNOWLEDGMENTS

I would like to thank my thesis committee for taking their precious time to review my thesis. I would also like to express my deepest gratitude to my committee chair, Dr. Jered Haun, for giving me the chance to work under his guidance and develop my research, analytical, and professional skills.

I would like to thank my lab mates, Maha Rahim, Xiaolong Qiu, Stephanie Pearlman, and Dweep Jhaveri. I would also like to thank my friend Alessandro Rossetta for helping me in writing the code and my friend Neto Sosa for his guidance on my dissertation.

ABSTRACT OF THE THESIS

Measuring Biomechanical Properties of Cancer Cells Using a High-Throughput Microfluidic Platform and Their Correlation with Surface Rheology and Internal Elasticity

By

Bahar Mousapour

Master of Science in Biomedical Engineering

University of California, Irvine, 2016

Assistant Professor Jered B. Haun, Chair

Biomarkers are intended to provide critical information to characterize the type/severity of the cancer, with the ultimate goal of providing information about treatment. However, their use in diagnostic applications is limited because they require the expensive and time consuming use of molecular probes. By using a technique that is label free and requires a simple and inexpensive microfluidic chip, we can capitalize on acute phenotypic differences that result from overexpression of glycoproteins that change the surface rheology of cells. Previous studies have shown that metastatic tumors overexpress bulky glycoproteins such as MUC1 which contributes to cancerous cell growth, adhesion, and survival. In our study, we quantified MUC1 expression in various cancer cell lines using flow cytometry and correlated this expression with the ability of cells to deform under shear forces during deformability cytometry experiments. Comparing the deformability data of cells from the same cell lines but with different levels of MUC1 expression provided compelling evidence that surface rheology effects can be captured using this technique. It has also been shown that the nucleus plays an important role in determining cell

deformability vis-a-vis internal elasticity. Therefore, we also measured the nucleus size of these cell lines with fluorescence microscopy and compared the area of the nucleus to the area of the cytoplasm. Comparing the ratio of these two measurements in each cell line with the deformability values confirmed that nucleus size is indeed the key factor determining cell elasticity and must be accounted for when considering deformability and MUC1 expression.

INTRODUCTION

What is cancer?

Cancer is a disease in which some cells lose the ability to properly manage cell division. These cells will grow and divide unchecked and form a tumor. Over time, these tumors will shed cells that will find their way through blood stream to invade other tissues and form secondary tumors. Secondary tumors are genetically similar to the original tumor even though they form in different body parts and organs. Healthy somatic cells are very specific depending on which part of the body they function in. For example, lung cells have a different structure than liver cells. On the other hand, cancer cells have a more general structure that allow them to survive in different organs. [1] Cancer is a universal disease that affects people from all demographics and age groups.

Cancer diagnosis

Doctors use a combination of screening tests such as blood and urine tests with imaging procedures to determine whether a patient has cancer and to determine how much the cancer has spread [2]. In screening tests, physicians look for certain proteins in blood, urine, stool samples, and tissue samples. These proteins of interest are produced by cancer cells or by normal cells responding to a malignant cancer and are referred to as tumor markers. The presence of tumor markers along with the tissue biopsy is the main tool for doctors to diagnose cancer. [3] In biopsy, part of the tissue is removed and sent to a pathology lab for more detailed information about the genetic and molecular makeup of the cells forming the tumor. Radiology procedures can also be used to create three-dimensional images of the inside of the body to show the presence and location of the tumor. [2]

Cancer therapy

Different therapies are available for cancer treatment. After considering the type of cancer and the stage of the disease doctors will decide on the appropriate therapy.

- **Surgery:** can be performed in different ways; invasive methods involve cutting into the body and to the tumor site to remove the tumor tissue with a scalpel. For topical or surface cancers such as skin cancer or cervical cancer, non-invasive methods include cryosurgery, which is destroying the cancerous or precancerous cells with cold liquid nitrogen, and the use of laser beams to shrink the tumor and kill the cancer cells. Hyperthermia is also used to knock down the cancer cell using thermal energy. Photodynamic therapy, which is mostly used for skin cancer, utilizes drugs that only activate with certain lights. These drugs are absorbed by dangerous cells, and once light activated, they kill the cancer cells. [4]
- **Radiation therapy:** emission of high intensity and localized radiation such as X-ray or Gamma-rays leads cell DNA damage. This damage eventually causes cell death and finally tumor shrinkage. Doctors decide whether the patient needs radiation therapy or if therapy should be received before, during, or after the surgery. Radiation sources can be placed outside or inside the body. Either of these two methods have side effects since radiation kills cells indiscriminately and both cancerous and non-cancerous cells die. [5]
- **Chemotherapy:** receiving drugs through intravenous (IV), injections, oral pills or capsules, and topical creams for external use; these drugs kill any cells as they divide. Therefore, fast growing cells are killed preferentially. This includes cancer

cells and fast growing healthy cells such as hair follicles, blood cells, immune cells, and cells that line the GI tract. This therapy does not have the same effectiveness for everyone because of genetic reasons. Side effects may also vary between patients but they involve the loss of fast growing healthy cells and lead to fatigue, mouth sores, nausea, and hair loss. [6]

- **Personalized Medicine:** also called precision medicine which goes beyond the type of cancer that the patient has and where it is located. This new treatment is based on the knowledge from recent research digging deeper into the cause of the disease and identifying the genetic factors associated with it. Cancers arise from a combination of some genetic failures that lead to out-of-control cell growth. Therefore, every patient tumor structure and genetic makeup is unique. This uniqueness is why a patients respond so differently to therapies. This difference is seen both in recovery and in the side effects that are present. [7]

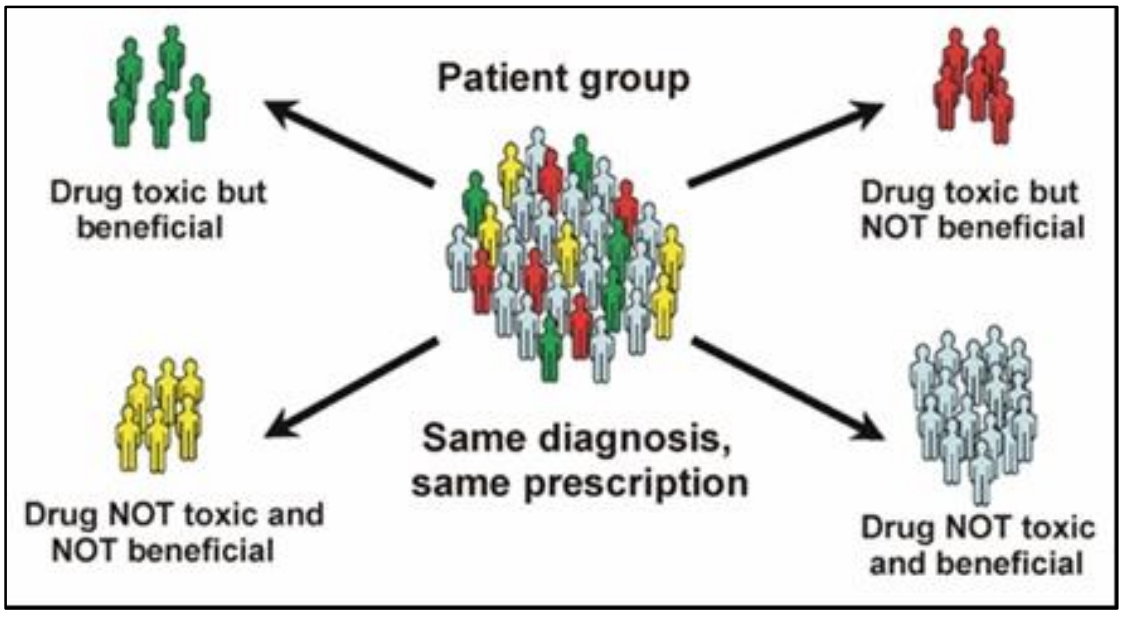

Figure 1-Different response to the same therapy [8]

This being said, oncology field has moved towards treating the person rather than the disease based on identifying the genetic profile of a tumor [9]. This selective therapy offers a patient the best treatment for their specific tumor. Personalized medicine is leading to higher recovery rates and less side effects.

Personalization could be in the form of examining someone's cancer to verify a certain treatment will be effective, finding out if a patient can handle a specific medicine by analyzing their genetic profile, or even assessing the risk of developing cancer by looking for genetic mutations. [7]

Each person not only has a unique personality but has a unique genome too. Because cancer is tied to genetics, every cancer patient's illness is also unique. Researchers see the future of cancer treatment in tailoring the therapy to the patient's individual needs. One of the first cancers that researchers trialed precision medicine in was lung cancer. In a study performed in 2007, clinicians used targeted drug therapy to aim for EGFR, the gene responsible for growing and dividing of the cells, hoping to stop the tumor growth. After gathering the patients' genetic information, results showed that over 70% of the patients that have a specific mutation in EGFR responded to this therapy versus 1.1% for the patients without that mutation. [9] The key to personalized cancer treatment is studying the patients' individual genome to find the weak spot of their cancer and designing drugs to target those weak spots.

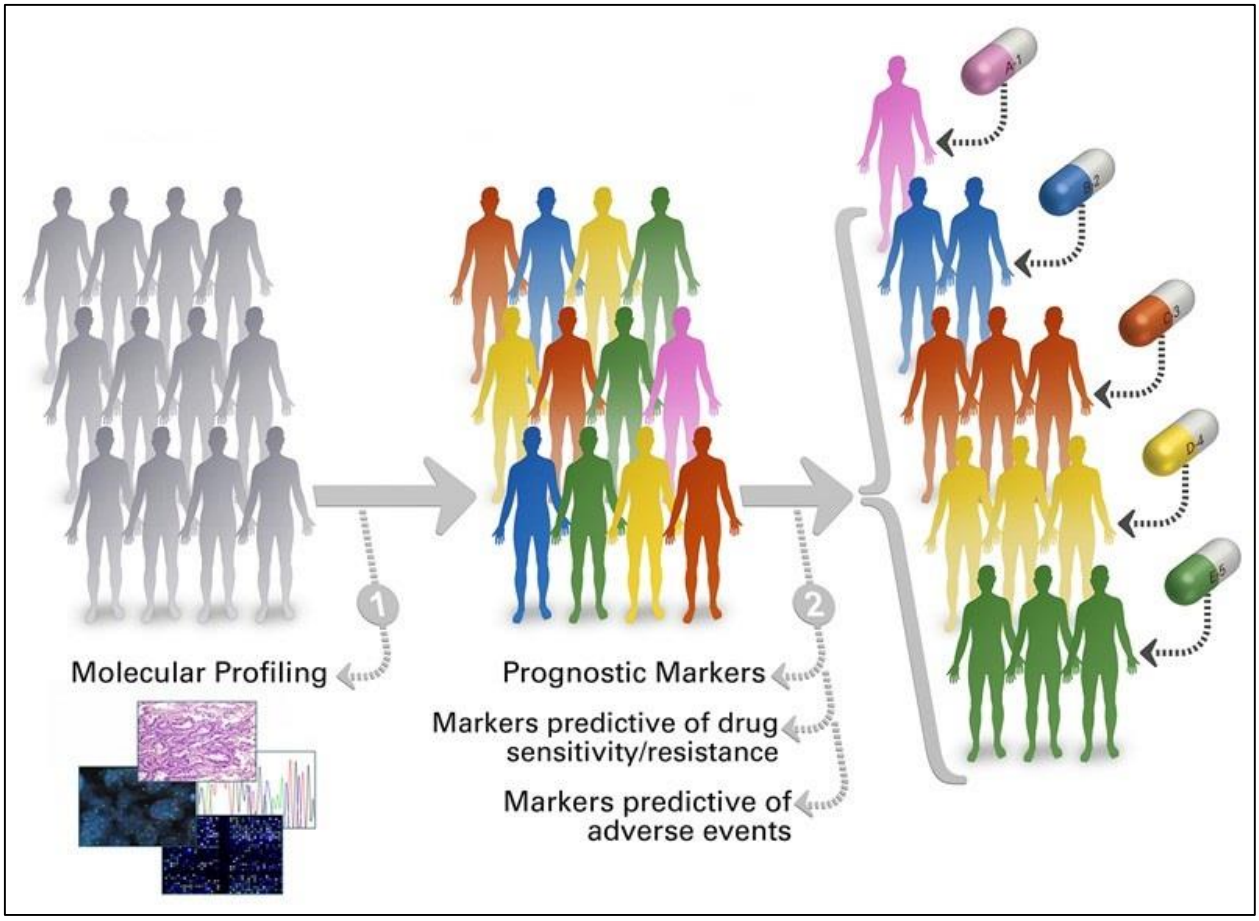

Figure 2- Personalized Cancer Therapy [10]

Microfluidics in Cancer

Microfluidic is an early stage technology used for manipulating and processing small amount of fluids in the range of milliliters to picoliters. [11] Microfluidic platforms are composed of small dimension channels with features from 10 Micrometers to 1 millimeter and have the capability to integrate multiple chips with different functions similar to electronic chips. [12] The advantages of microfluidic platforms such as their small size, low cost, assay times, low material costs, high throughput, and potential for built in automated analysis makes it a promising technology in many scientific fields including Oncology [11].

Key microfluidic technology that has been developed for cancer cell detection, characterization, and separation is mostly based on the biophysical properties of cancer cells. The most popular approach includes magnetic activated cell sorting platforms that detect and separate cancer cells using magnetic beads binding to targeted antibodies on the surface of the cells and allow for further manipulation and processes post-capture. Size-based microfluidic platforms use the size of the cells to separate the cancer cells without knowing the biochemical characteristics. This approach is useful to detect circulating tumor cells (CTC) since they are normally bigger than other cancerous cells. On-Chip Dielectrophoresis exploits the polarity of the cells using a non-uniform electrical field to separate cells based on their charge. Cell size, membrane profile, and cytoplasm electrical properties are the elements that determine a cell's polarity. [13]

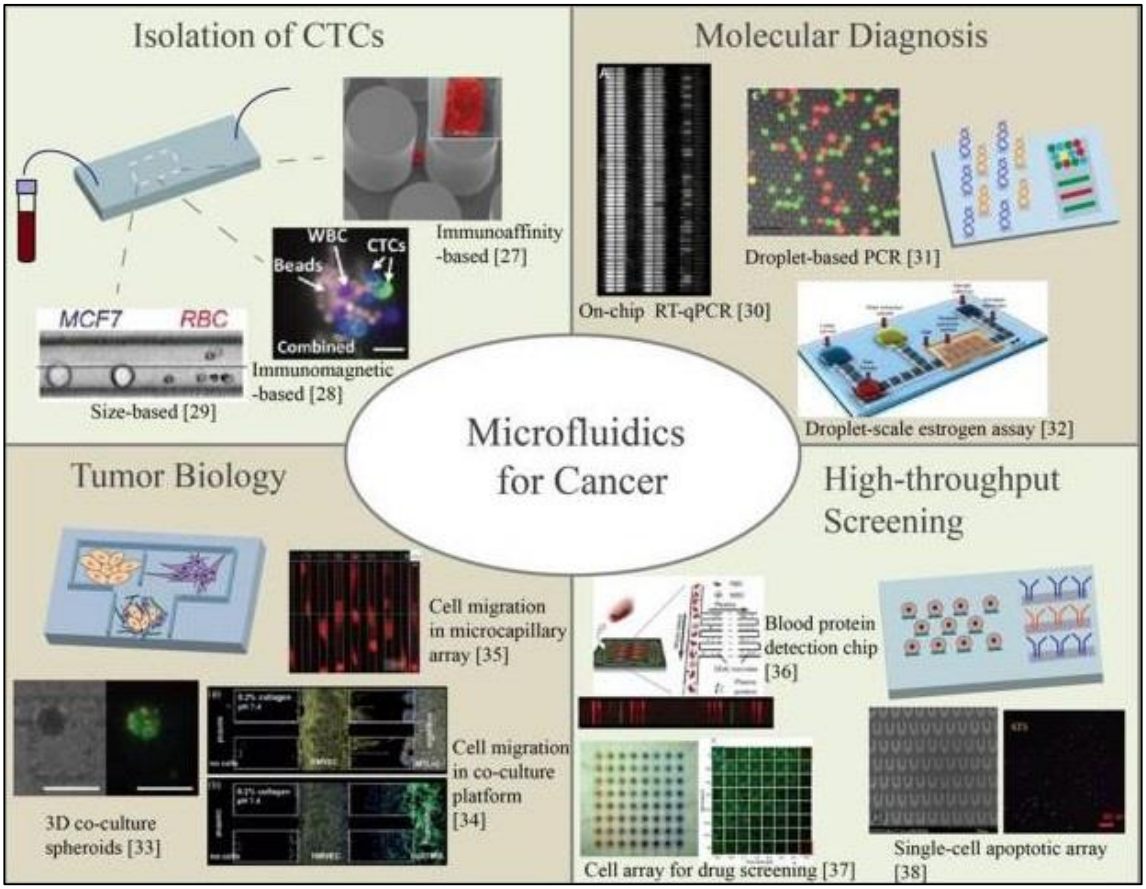

Figure 3- Microfluidic technology applications in cancer [14]

Project Overview

The first part of this work focuses on the surface rheology and nucleus size of cancerous cells. These are two important elements that contribute to the cell's deformability. In the next chapter, I explain the reasons we focused on these two elements and how they were quantified in all the cell lines included in our study. The second part of this work focuses on the developed microfluidic platform that was used for deformability measurements of the studied cell lines.

Chapter 2

Surface Rheology and Nucleus size; Key Factors to Cell Mechanics

2.1. Surface Rheology (MUC1 Expression)

2.1.1. Background

Mucin1 (MUC 1) is an extracellular protein that is glycosylated to the membrane of epithelial cells and act as a selective barrier at the surface of the cells. Transformed expression levels of these proteins are associated with the cancer development, cell growth rate, and differentiation. Studies have shown abundant and large glycoproteins are often found in circulating tumor cells. This suggests a link between bulky glycoproteins and intrusion metastasis, as well as a link with protection mechanisms of cancerous cells. Anti-adhesion effects of mucins help with dissociating the cancer cells from the original tumor mass. The adhesive effect of mucin also benefits cancerous cell in facilitating attachment to endothelia for invasion. Furthermore, mucin aids cancerous cells in remaining undetected from immune surveillance. Atypical expression of MUC1 changes the surface rheology of the cells. Our lab is interested to learn if the MUC 1 expression content has any effect on cell deformability. [15]

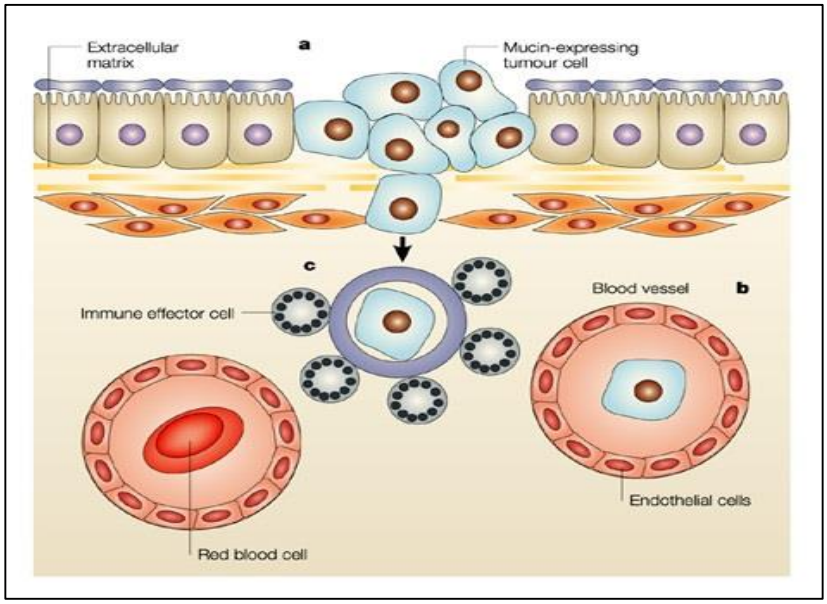

Figure 4- Mucin effects in cancer [15]

2.1.2. Material and method

To quantify the MUC1 expression content of our cell lines of interest, we used antibodies tagged with fluorescent dyes that bind specifically to MUC-1 antigens and used flow cytometry, a technique which uses light to quantify the the fluorescent dyes and therefore the levels of MUC-1 expression. In this technique cells flow through a channel and pass through an excitation wavelength which excites any fluorophores bound to their protein targets. The fluorophores then emit light that is detected by sensors. This fluorophore data is collected and compiled to provide a comprehensive histogram of the sample. [16]

To perform flow cytometry cells are counted with a Hemocytometer. 100,000 to 500,000 cells are aliquoted in 3 samples. The first sample is for background control using a nonbinding monoclonal antibody (rat anti-mouse IgG1, clone A85-1, BD Biosciences, San Jose, CA). The second sample is incubated with mouse monoclonal mucin1 antibody that

targets a tandem repeat of MUC 1 of human origin (sc-7313, VU4H5, Santa Cruz Biotechnology) [17]. Finally, the third sample is incubated with MUC 1 (mouse IgG_1, clone M01102909, Fitzgerald Industries International, Acton, MA). Cells are washed with 500 µl of PBS+ to get rid of excess media and resusupended in 149 µl of PBS+. 1µl of primary antibody (Santa Cruz and Fitzgerald) is added to the second and third samples and left on a rotating tray to incubate for 30 minutes. Samples are washed twice with 500 µl PBS+ to remove unbound floating antibodies. Then 1µl of secondary antibody (IgG1) is added to all three samples and placed in ice for 30 minutes. The samples are vortexed 3 times every 10-minutes. At this point, the secondary antibody conjugated with a Fluorophore (FITC) is attached to primary antibodies. This secondary antibody serves to amplify the signal of bound primary antibody. Finally, samples are washed with PBS+ three times after incubation and placed into flow cytometry tubes.

2.1.3. Results and discussion

In this part, Mucin 1 expression detected with Fitzgerald and SCBT antibodies are presented. Besides the cell lines listed in the table below, we also measured Mucin-1 expression for various types of MCF10A, MDA-MB-231, and MCF-7 cell lines. In addition to their wild-type, we have modified versions of them with transfected genes in order to express different levels of Mucin-1. For MCF10A and MDA-MB-231, and MCF-7 we have the induced MUC1 type to express higher level of this protein while for MCF-7 we have the additional knock-out (KO) version to express lower level of MUC1.

Table 1- List of studied cell lines for flow cytometry experiments

Hela	Cervical cancer
SKOV3	Ovarian cancer
SKBR3	Breast cancer
HCT116	Colon cancer
H1650	Lung cancer
A431	Epidermoid carcinoma
MCF10A	Breast cancer
MDA-MB-231	Breast cancer
MCF-7	Breast cancer

Table 2- MUC1 expression detected with Fitzgerald and SCBT antibodies

Cell Line	HeLa	SKOV3	SKBR3	HCT116	H1650	A431
Fitzgerald	2745.513	2094.48	709.8	18.5	8086	44.3
SCBT	104.013	15.4	64.8	8.4	16.25	4.04

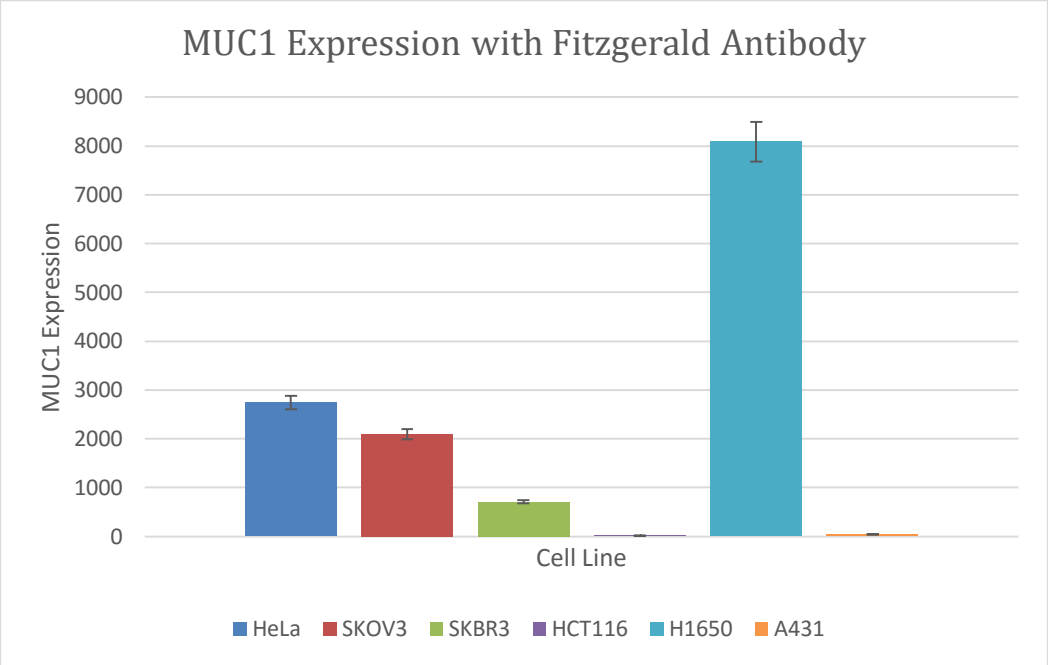

Figure 5- MUC1 expression detected with Fitzgerald antibody for the studied cell lines

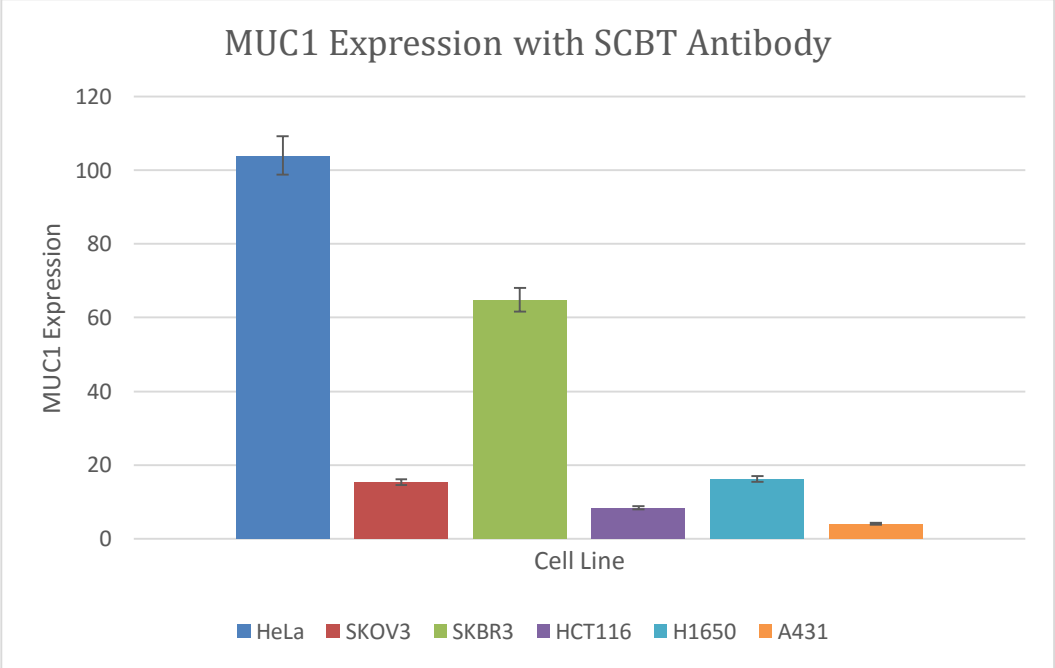

Figure 6- MUC1 expression detected with SCBT antibody for the studied cell lines

Table 3- MUC1 expression for various types of MCF10A, MDA, MCF7

Cell Line	MCF10A-WT	MCF10A-MUC1	MDA-WT	MDA-MUC1	MCF7-WT	MCF7-HE	MCF7-KO
Fitzgerald	2278	18540	206.67	445	3035.6	3244.56	356.16
SCBT	16.45	16845	4.18	3.45	28.1	54.075	15.15

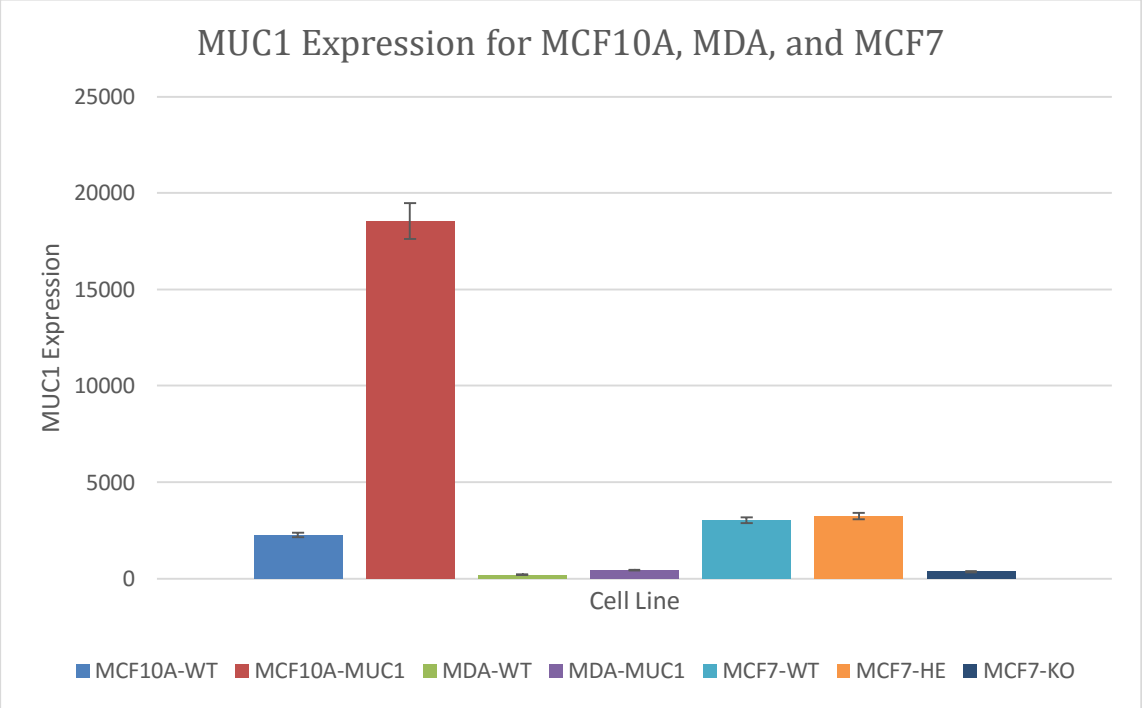

Figure 7- MUC1 expression for various types of MCF10A, MDA, MCF7 detected with Fitzgerald antibody

2.2. Nucleus size

2.2.1. Background

Previous studies on nucleus mechanics show there is much more deformation response from cytoplasm than nuclei when exerting mechanical force on cells using micropipette aspiration. This suggests that the nucleus is a more rigid structure compared to the cytoplasm. Furthermore, labeling the nucleus envelope with Fluorescent markers revealed that the nucleus envelope acts as a solid-plastic allowing it to stretch out and

resists shear force induced by micropipette aspiration. [18] Studies by *Di Carlo* and colleagues show that nucleus size is a dominant factor in cell deformation which is our main motivation to gather information about the nucleus size of our studied cells [19].

2.2.2. Material and Method

2.2.2.1. Nucleus Imaging

We use Hoechst dye, a type of blue fluorescent dye to stain the DNA. Stock solution is made in DPBS to a final concentration of 1mg/ml from which working solution is made at 5µg/ml concentration since Hoechst dye concentration for live animal cells should be between 0.2µg/ml to 5µg/ml. 1ml of working solution is added to 1ml of cells in the media and incubated for 20 minutes in 37°C. After incubation, cells are spun down and washed with PBS+ three times to remove excess dye. 30µl of washed cells are then placed between two glass sides. For imaging we used a Hoffman Modulation Contrast by Nikon to take pictures of the whole cell in bright field and also the stained nucleus using the DAPI filter with a 60X oil immersion objective lens.

2.2.2.2. Data Analysis

Image J software was used for measuring the cell and nucleus area having the pixel size for a 60x objective, 7.770 pixels/µm, and set this as the scale value.

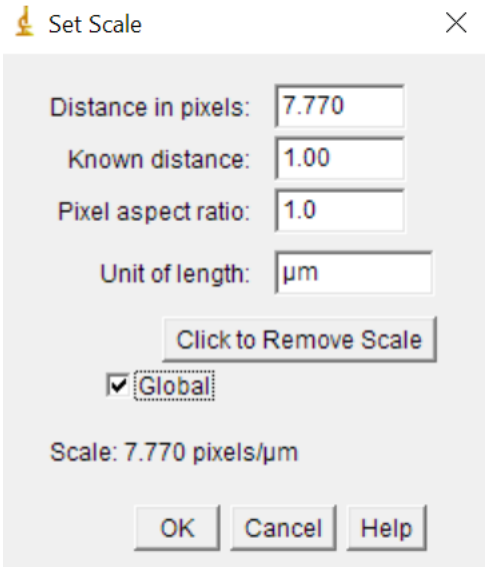

Figure 8- Set Scale window in Image J

Images of the whole cell and nucleus saved in jpeg formats and then the area is marked using the "freehand selection" tool in image J and then measured.

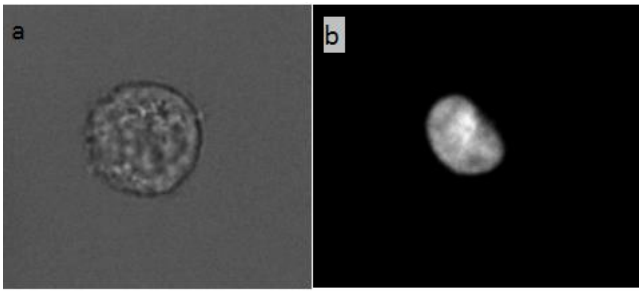

Figure 9- (a) cell image, (b) nucleus image

Having the cell and nucleus area, we can now calculate the ratio of the nucleus to the cell area to know how much of the cell is being occupied by the nucleus.

2.2.3. Results and Discussion

In this section, cell and nucleus area is presented along with the ratio of nucleus to the cell area for the cell lines listed in the table below.

Table 4- List of the studied cell lines included in imaging study

Hela	Cervical cancer
SKOV3	Ovarian cancer
SKBR3	Breast cancer
HCT116	Colon cancer
H1650	Lung cancer
MCF10A	Breast cancer
MDA-MB-231	Breast cancer
MCF-7	Breast cancer

Table 5- Cell area, nucleus area, and the ratio of nucleus to total area for the studied cell lines

Cell Line	**HCT116**	**SKBR3**	**H1650**	**SKOV3**	**HeLa**	**MCF10A**	**MDA-MB-231**	**MCF-7**
Total Area	125.064	477.763	367.744	303.946	262.4823	253.205	338.068	302.615
Nucleus Area	58.965	175.722	109.023	103.927	100.6949	90.612	136.389	115.976
Nuc/Tot Area	0.479	0.379	0.304	0.350	0.3851	0.360	0.406	0.388

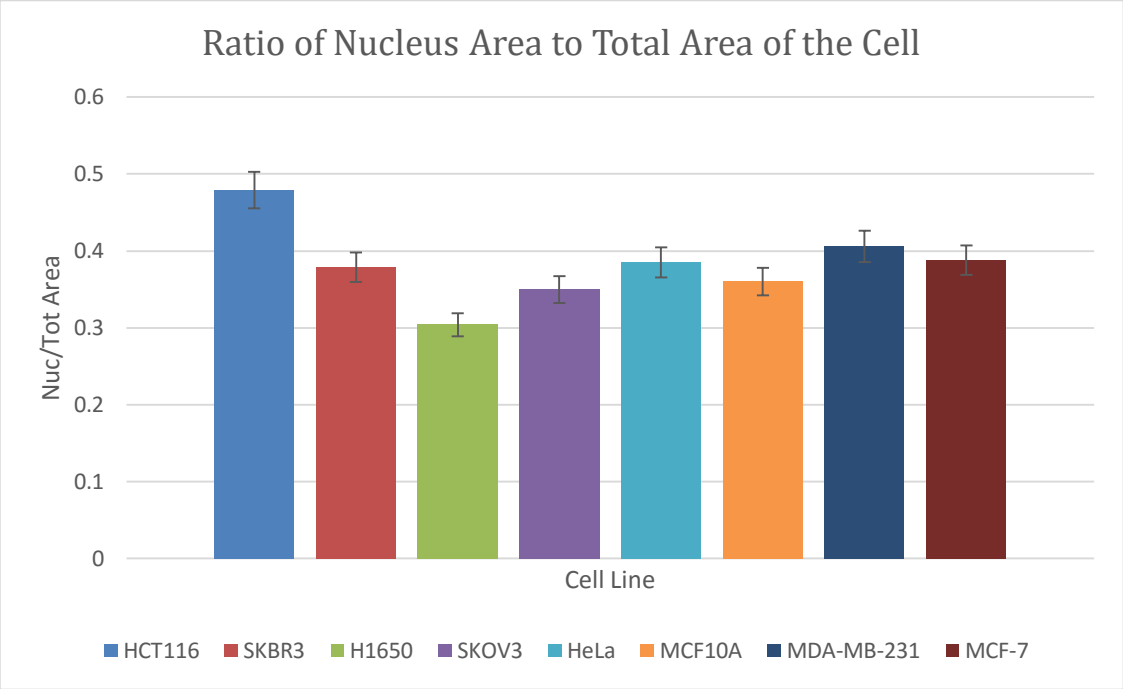

Figure 10- Ratio of nucleus to the total area of the cells for studied cell lines

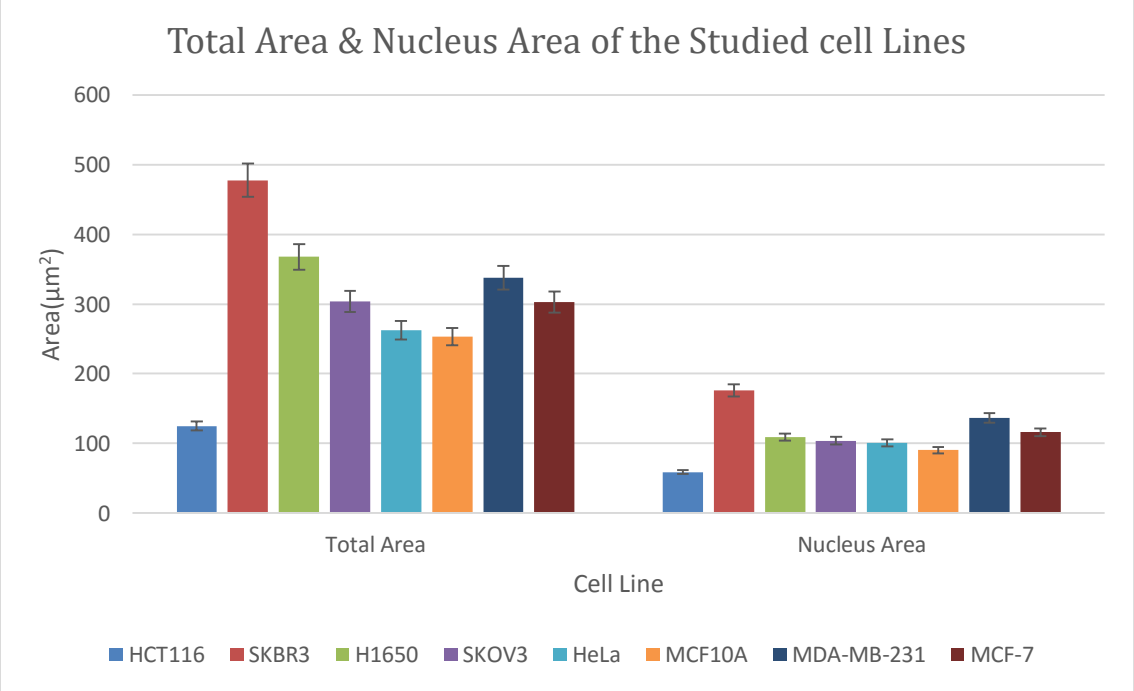

Figure 11-Total area vs. nucleus area of the studied cell lines

Chapter 3

Study of Shear Stress Effects on Cell Mechanics with Microfluidic Platform

3.1. Background

Cell mechanical properties reveal a lot of information about the underlying molecular structure of the cell and these detectable features can be used as label-free biomarkers to rule out the cell state and disease [19]. As mentioned before, molecular and genetic alteration can lead to phenotypic changes in cells which in turn induce changes in their mechanical behavior. This change in mechanical behavior is the main focus of our study. Heterogeneous populations of cells are usually found in tumors and it is important to distinguish these populations to obtain accurate information. Single-cell microfluidic platforms allow us to study heterogeneous populations in a high-throughput manner. This is a fast and low-cost tool to detect phenotypic changes. Recently Di Carlo and colleagues designed a microfluidic device that can measure cell deformability [20] which our lab improved upon for our specific application. There are two main parameters that we included in the device design; laminar flow and inertial focusing of the cells. Laminar flow happens when fluid flows in parallel layers without lateral mixing and particles in fluid travel in orderly straight lines parallel to the pipe wall [21]. The Reynolds Number (Re) can be used to determine whether the flow is laminar (Re <2300), transient (2300< Re <4000) or turbulent (Re >4000). The Reynolds number is a dimensionless quantity which is defined as the ratio of inertial force to viscous force or how fast the fluid is moving relative to how viscous it is [21].

$$Re = \frac{Inertial\ Forces}{Viscous\ Forces} = \frac{\rho v L}{\mu} = \frac{vL}{\vartheta}$$

In which v is the mean velocity of a particle with respect to the fluid, L is the length of the channel, ρ is density of the fluid, μ is dynamic viscosity, and ϑ is kinematic viscosity.

In addition to laminar flow, we used an inertial focusing channel to place the cells in the center of the channel and away from the walls. This also helps reduce the pressure inside the device. Extra fluid is removed by two siphoning channels. The mechanism of inertial focusing relies on the hydrodynamic forces exerted on particles traveling along the channel of the device. These forces move the particles towards the center of the channel [22].

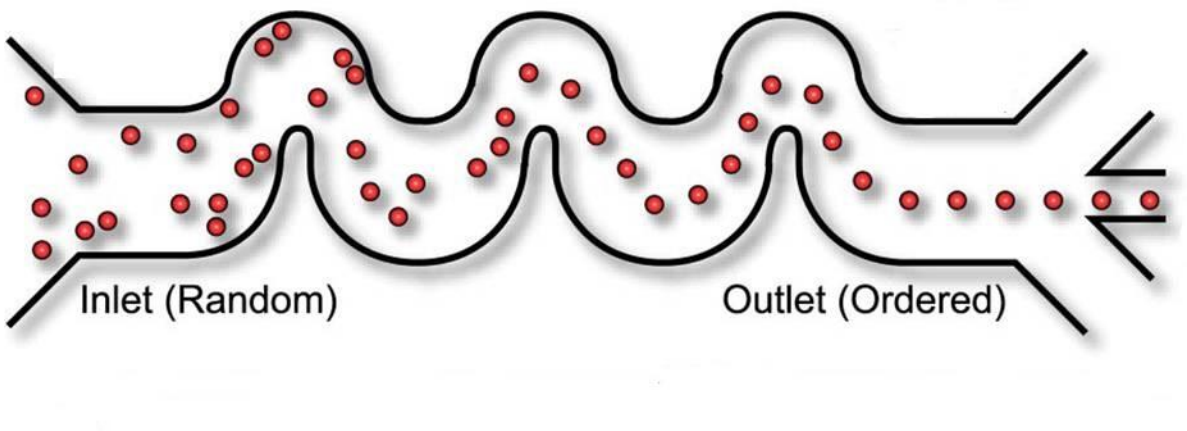

Figure 12-Inertial focusing effect [23]

3.2. Material and method

3.2.1. Device Design and Production

The device design was done by Dweep Javaheri using AutoCad software and it consists of three inlets, three outlets and two inertial focusing channels (Figure 6). The height of the channels is 45 µm and the total device length is 2.62 cm. The width of the angled siphoning channels and linear channels are 35 µm and 67 µm respectively. The diameter of the device openings is 8 µm. Cells will move towards the center as they travel along the first and longer inertial focusing channel while excess buffer move close to the walls of the channel, this excess buffer is then siphoned out by the two siphoning channels. As the cell stream moves past the T-junction they go through a second inertial focusing channel to get focused at the center of the channel again which in turn merges with two perpendicular buffer flows.

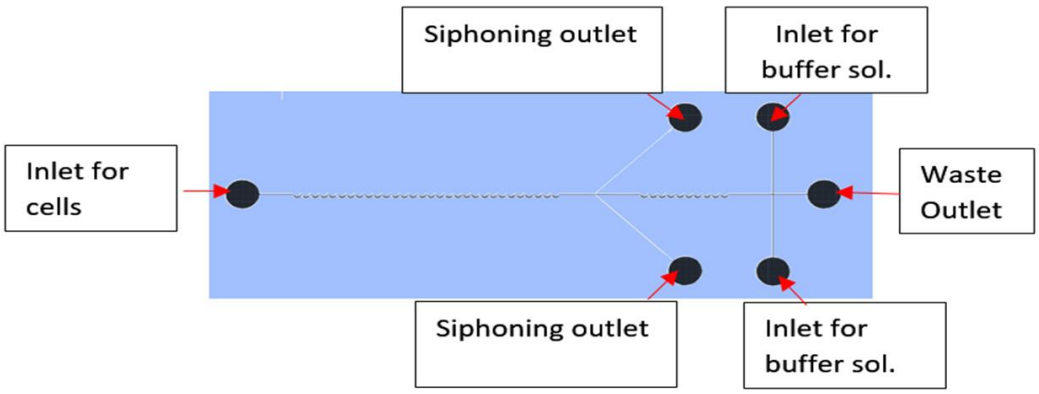

Figure 13- Device design

Using the design above, a photo mask of 30 µm resolution was prepared by Finleline Inc. The mask was then used to create the silicon wafer by a technique called photolithography which can create extremely small patterns.

To make the PDMS device, polydimethylsiloxane and curing agent is mixed at the ratio of 9:1 respectively and poured over the silicon wafer, then the wafer is placed in a vacuum desiccator to remove air from the uncured PDMS. This process is complete when all air bubbles have disappeared and no new bubbles are forming. The next step is putting the wafer in the oven at 65°C for 12 hours in order for the PDMS to cure. Once cured, the wafer is left out in at room temperature for an hour to cool down before the mold is cut out and openings are punctured. The device is cleaned with an air gun and tape to get rid of any unwanted particles. The PDMS device is then plasma bonded to a glass slide. Next, Plastic tubing with the needle gauge 30 and the inner and outer diameter of 0.25mm and 0.75 is inserted. The length of the tubing for all the 3 inlets is 37 cm, for siphoning outlets 50 cm, and for the outlet it is 25 cm. These lengths are calculated based on the time required for the fluid to enter and exit the device without creating too much pressure. Syringes and needles that used are from BD Sciences with the following specifications; 10 ml syringes with 1ml tip used along with needles of 0.25 mm outer diameter and a 0.06mm inner diameter. Finally, the device is flushed with DI water at a 500 µl/min flow rate for 20 minutes. This step ensures there is no leakage and also washes out any PDMS residue in the channels.

3.2.2. Experiment setup

The device is placed under an inverted microscope. Using a 20x objective, the microscope is focused on the T-junction where all 3 streams merge. For our experiment we used high speed camera known as Phantom camera v310 which connected to the scopes external port. The camera was in turn connected to a computer and operated through Phantom Camera Control software. The Phantom uses 0.63x lens which allows for better

focus on the cells. The resolution is set to 128x128 and the highest frame rate and maximum exposure time available for this resolution is 120171 fps and 7.63 µs respectively. 2 pumps are connected to the device, one for cell injection at 500 µl/min and the other one for 2 buffer flow injections at 350 µl/min. The waste is collected in a glass beaker.

Figure 14- Experiment Setup

3.2.3. Data Analysis

Cells get more squeezed as they pass through the hydropipetting junction where the cell flow meets 2 opposing buffer flows. Deformability values vary in different regions of the device. To understand this, we divided the hydropipetting junction in 3 sections and analyzed the deformability results in these 3 locations.

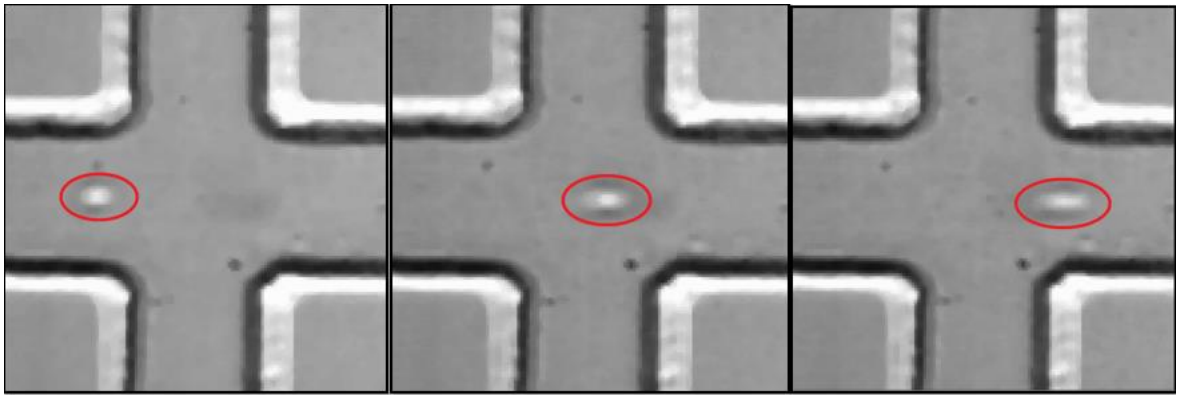

Figure 15-Cell gets squished as it passes through the hydropipetting junction

In this section the development and the functioning of the code that was used for data analysis will be described. Before we started this project, previous data analysis results were obtained by passing the raw data, from the acquisition camera, through multiple and different software programs in a non-homogenous way. The need to make data analysis process more efficient and user-friendly drove us to the development of a custom MATLAB code or data processing.

The MATLAB code was written into a *script* file using the *cell* compilation mode which breaks down the algorithm into small parts. In this way the user can directly run the whole code or actively and selectively run a specific portion of the code to accomplish a single function without reloading the entire dataset.

Having set the pixel-size (which was fixed at a value of 1.56 μm in all the experiments we performed) the code gives the option to select the *.avi* video to analyze. After the video is loaded, data is shaped into a 3D matrix and stored. The first operation on the data is a de-noise function which consists of the "*salt and pepper"* noise removal: a median filter (*medfilt2*) is used to smooth images pixel values. Images are then converted

into *grayscale* (*mat2gray*) and, after a contrast adjustment procedure (*imadjust*), all the images are shown to the user with the respective frame number – see Figure 9.

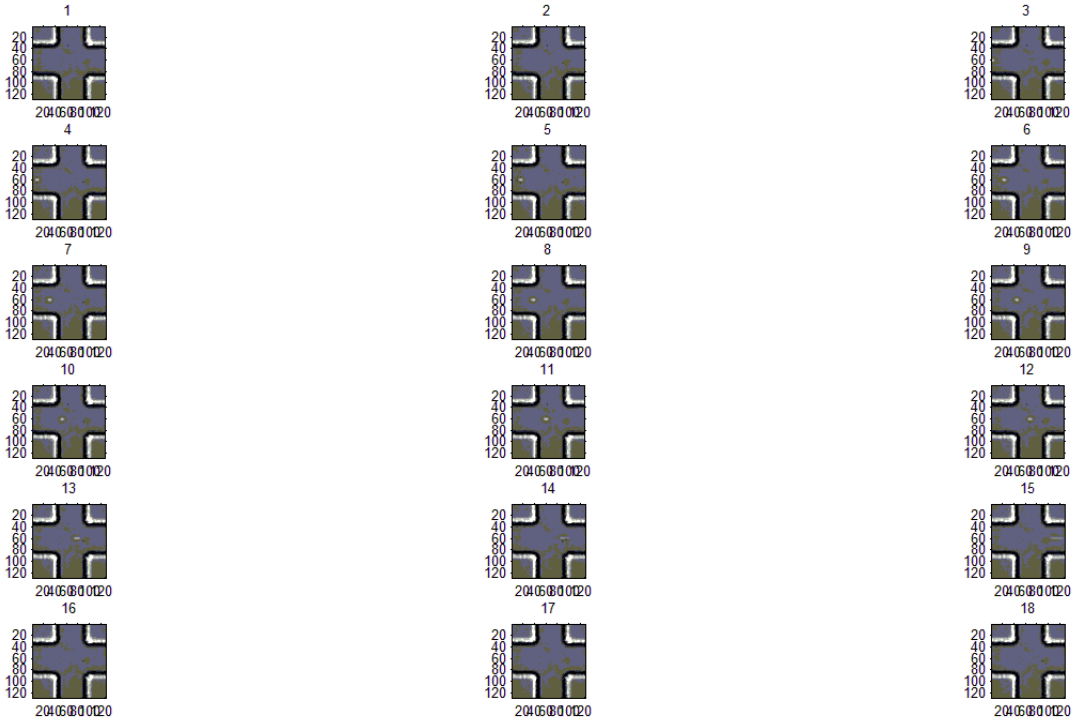

Figure 16-Grid visualization of video frames (x and y axes units are pixel numbers)

Video frames are presented to the user with a grid visualization. Using this approach, the user can simply zoom in and observe the exact location of the cell and then select the desired frames through a pop-up window (Figure 10), that appears at the same time as the grid. Up to four frames or four different moments of cell transition and distortion due to the microfluidic device action can be analyzed. Once the user has completed this step and

selected four frames the code allows the analysis of each single frame independently. We will now discuss the process for one frame only.

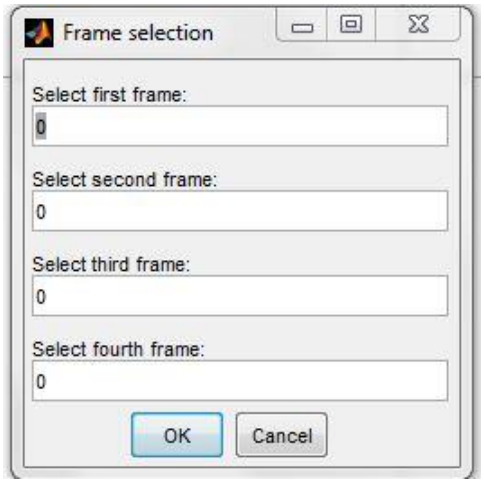

Figure 17- Dialog window for frame selection

At this time a selected frame is shown to the user (Figure 11A) and then the user will have to crop (MATLAB function *imcrop*) a region of interest (ROI) of the image in which a cell is present – Figure 11B.

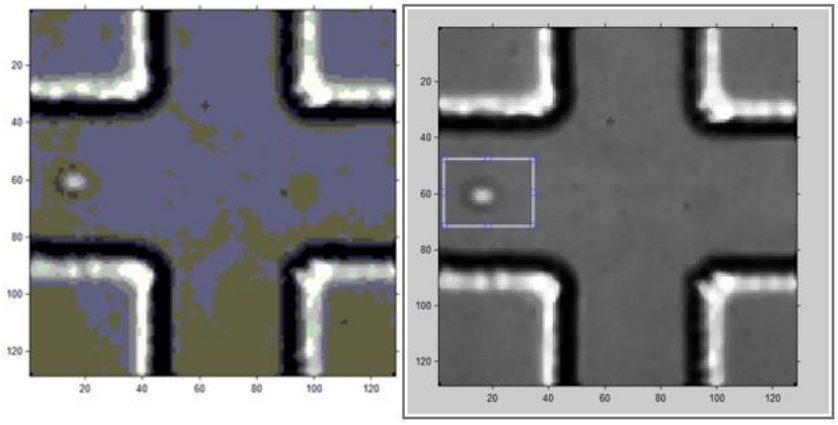

Figure 18- (a) selected frame, (b) crop function

That region of the image where the cell was present (Figure 12a below) is taken and transformed into a *binary* image (an image which pixel values are only 1 or 0) using a *Canny* edge filter – Figure 12b. the Canny edge detection algorithm looks for large pixel value differences between adjacent pixels to delineate object edges.

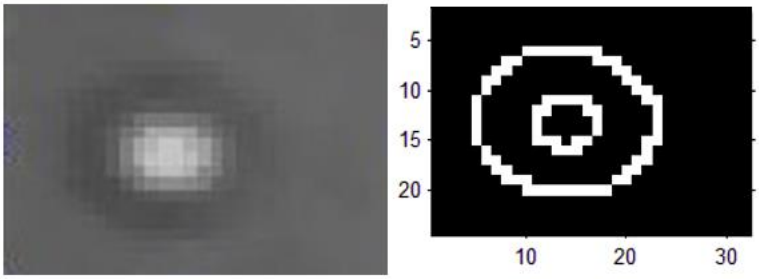

Figure 19- (a) cropped cell, (b) binary image of the cell

Through the pixel selection MATLAB function "*ginput*" the user can manually select four points of coordinates in the "edge" cell image – see example in Figure 13. By processing these x and y values it is possible to calculate cell dimension along the two main axis.

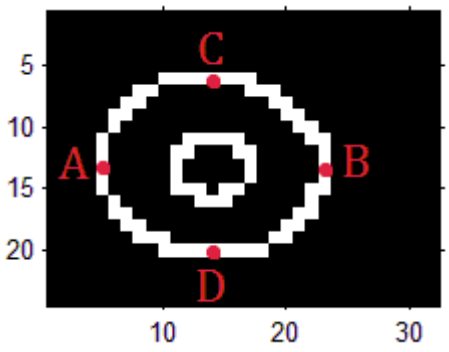

Figure 20- Selected points are the red dots marked by the letters A, B, C, and D

As we previously stated, the code performs the operation we described above for all the four selected frames and it also outputs the values of the cell main axis into an *Excel* spreadsheet

for further analysis. Using the formula below, a deformability value (D) can be derived having x and y dimensions of the cells.

$$\boldsymbol{D = \frac{X}{Y}}$$

3.3. Results and Discussion

In this section the results for all the cell lines that we studied are presented in a table and graph. Each experiment was repeated in three rounds in different days with different devices to ensure that the acquired data is accurate and independent of the tools.

Table 6- List of studied cell lines for deformability assay

Hela	Cervical cancer
SKOV3	Ovarian cancer
SKBR3	Breast cancer
HCT116	Colon cancer
H1650	Lung cancer
A431	Epidermoid carcinoma

For each cell line, deformability was measured in three locations. The closer the value is to 1 the more the cell is affected by shear stress. We discovered that each cell line has a unique deformability profile (see table1 and figure 14).

Table 7- Deformability values in three locations for different cell lines

Cell Line	SKOV3	SKBR3	HCT116	A431	HeLa	H1650
D1(Location1)	0.212	0.332	0.440	0.505	0.223	0.362
D2(Location2)	0.345	0.502	0.629	0.620	0.352	0.532
D3(Location3)	0.752	1.102	1.026	0.884	0.706	0.839

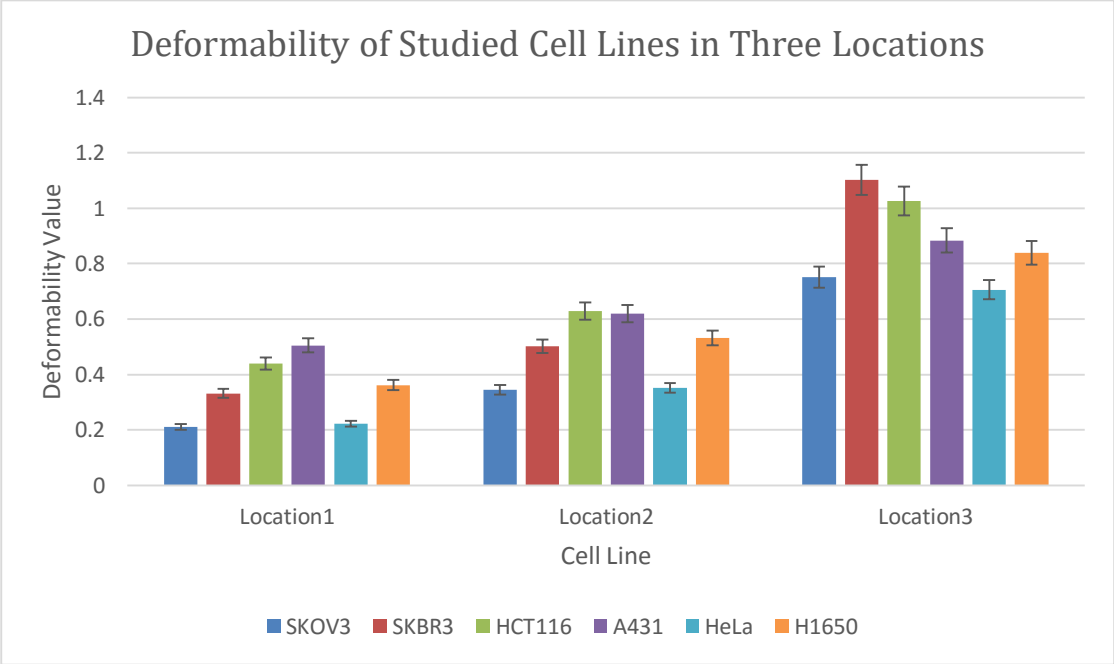

Figure 21- Deformability profile for studied cell lines

Next, we tested to see how different levels of MUC1 expression in the same cell line affects deformability under shear stress. Therefore, we studied three breast cell lines with different MUC1 expression; MCF10A, MDA-MB-231, and MCF7s. For MC10A and MDA-MB-231 we studied their wild-type (wt) phenotypes and increased MUC1 expression with a transfected gene. For MCF7, we studied both the wild-type and high MUC1 expression line, as well as a MUC-1 knock-out (KO) version. The results are shown in the following tables and graphs.

❖ ***MCF10A***

Table 8- Deformability values for MCF10A-WT and MCF10A-MUC1

Cell Line	MCF10A-WT	MCF10A-MUC1
D1 (Location1)	0.263	0.344
D2 (Location2)	0.387	0.499
D3 (Location3)	0.748	0.974

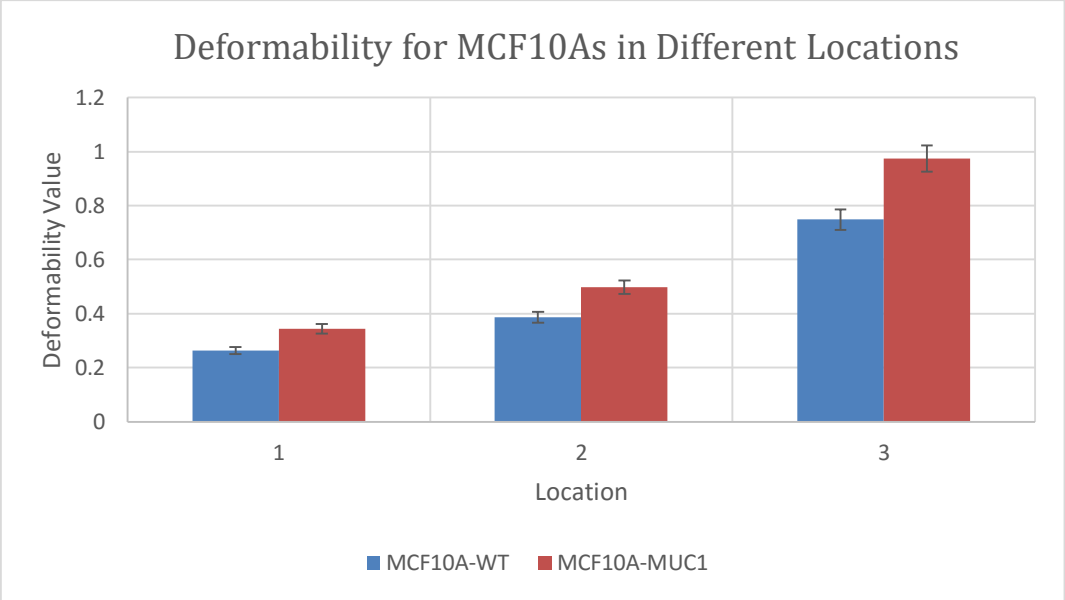

Figure 22- Deformability profile for MCF10A-WT and MCF10A-MUC1

❖ **MDA-MB-231**

Table 9- Deformability values for MDA-MB-231-WT and MDA-MB-231-MUC1

Cell Line	MDA-MB-231-WT	MDA-MB-231-MUC1
D1 (Location1)	0.206	0.224
D2 (Location2)	0.34	0.338
D3 (Location3)	0.616	0.723

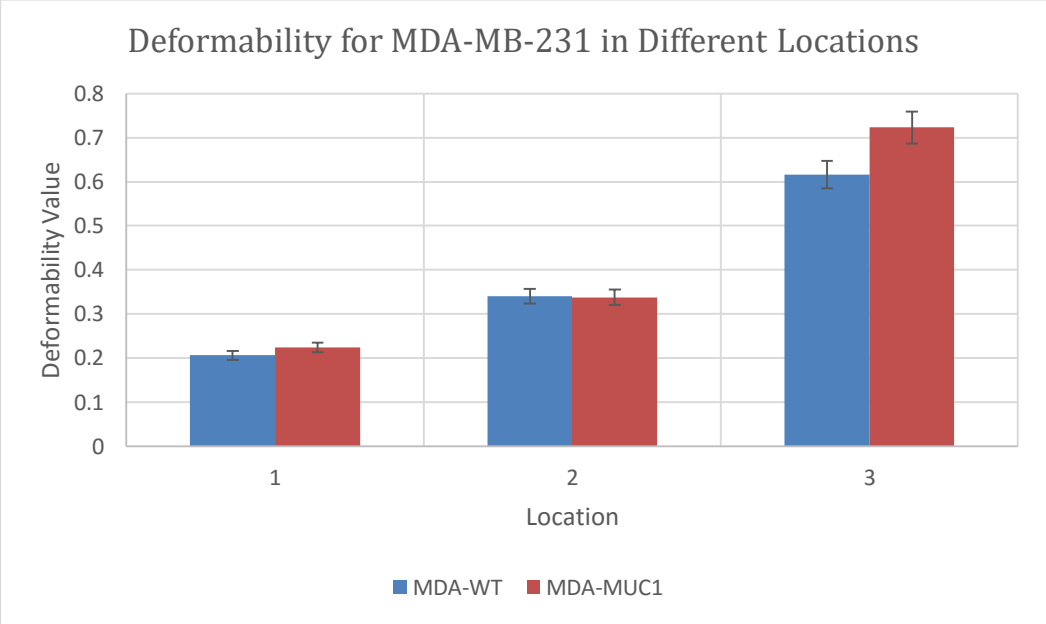

Figure 23-Deformability profile for MDA-MB-231-wt and MDA-MB-231-MUC1

❖ **MCF7**

Table 10- Deformability values for MCF7-WT, MCF7-KO, and MCF7-HE

Cell Line	MCF7-WT	MCF7-KO	MCF7-HE
D1 (Location1)	0.276	0.185	0.341
D2 (Location2)	0.411	0.282	0.480
D3 (Location3)	0.829	0.512	1.079

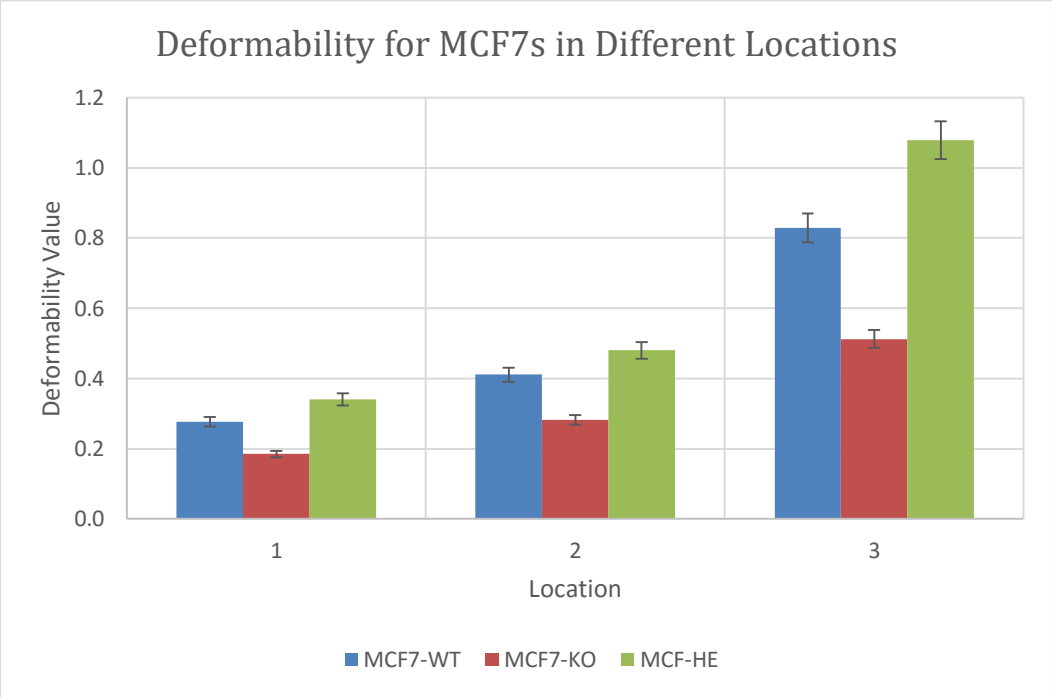

Figure 24- Deformability profile for MCF-WT, MCF7-KO, and MCF7-HE

Chapter 4

Summary and Future Direction

To test our hypothesis that Mucin-1 expression levels are correlated with the deformability rate under shear stress, we used cells with various MUC1 expression from the same breast cancer cell lines.

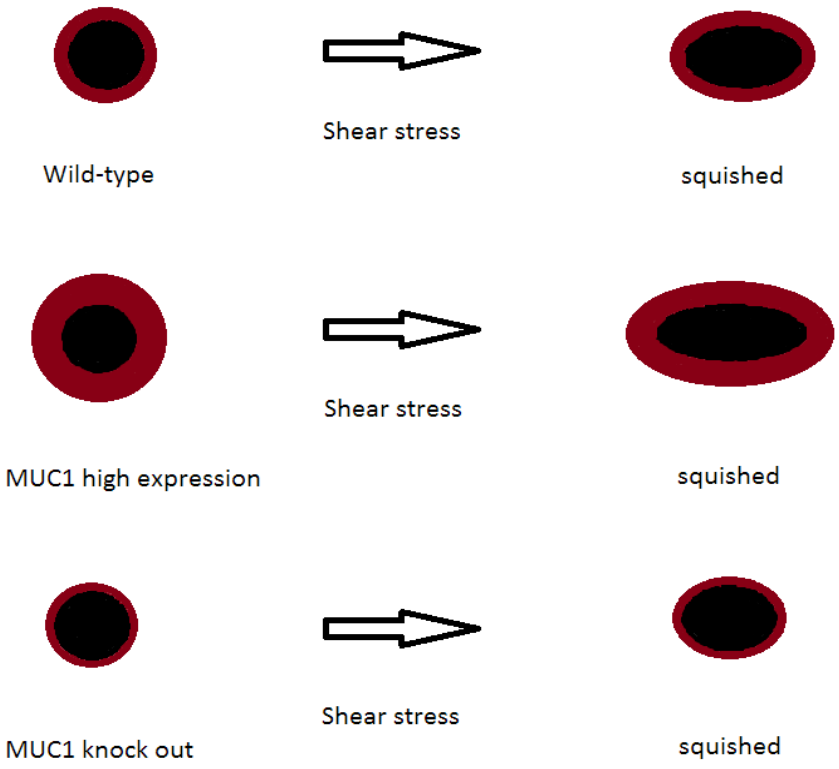

Figure 25 -Different levels of Mucin-1 expression and its effect on the deformability

Results show that increase in MUC1 expression in MCF10A, MDA-MB-231, and MCF7 cell lines results in up to a 30% increase in deformability rate. On the other hand, a decrease in MUC1 expression in MCF7 results in up to a 40% decrease in deformability rate. Since

Mucin-1 effects manifested the most at location 3, we plot deformability values at this location vs. Mucin1 expression with Fitzgerald and Santa Cruz antibodies separately for these cell lines to envision any trends.

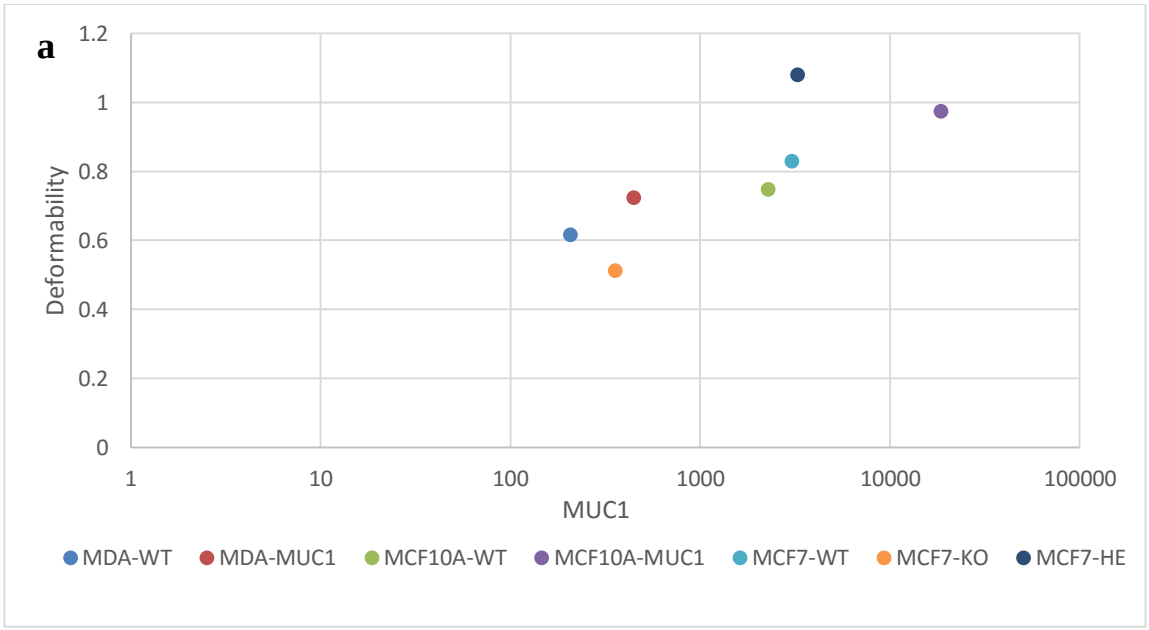

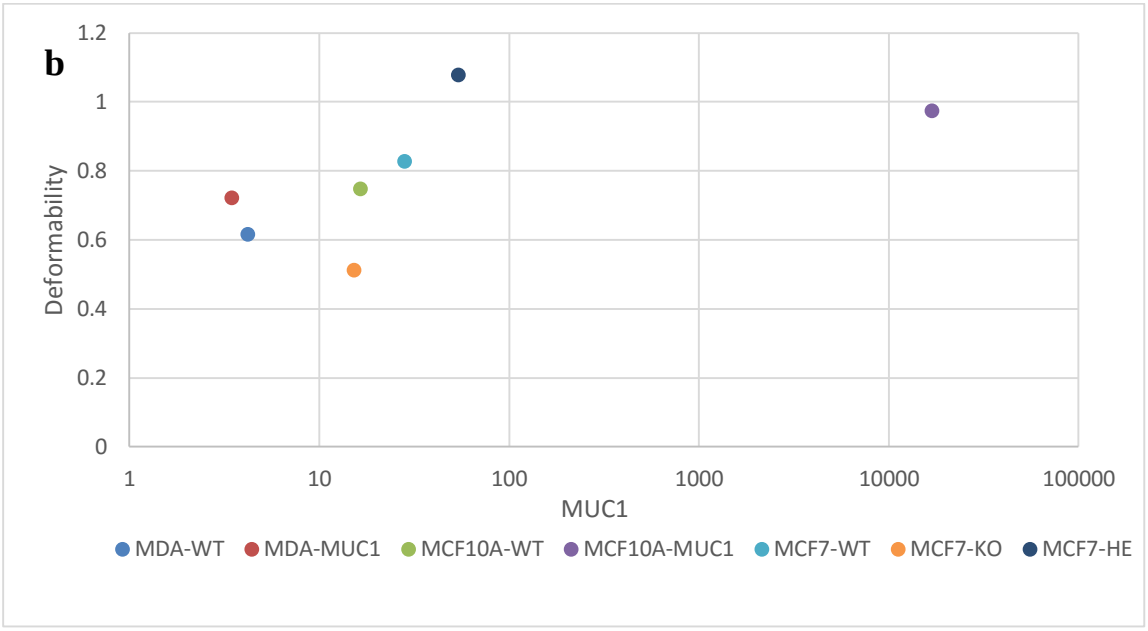

Figure 26- (a) Deformability Vs. MUC1 expression detected with Fitzgerald antibody, (b) Deformability Vs. MUC1 expression detected with Santa Cruz antibody

Based on the graphs above, it can be concluded that the Fitzgerald antibody is more predictive of deformability changes in respect to Mucin-1 expression than the Santa Cruz antibody because the Santa Cruz antibody reveals too low MUC1 intensity to discern between the different cell lines.

Furthermore, results show that each cell line has a unique deformability profile and these patterns can be used to obtain independent information about surface rheology and internal elasticity. These two main forces acting together determine the cell deformability.

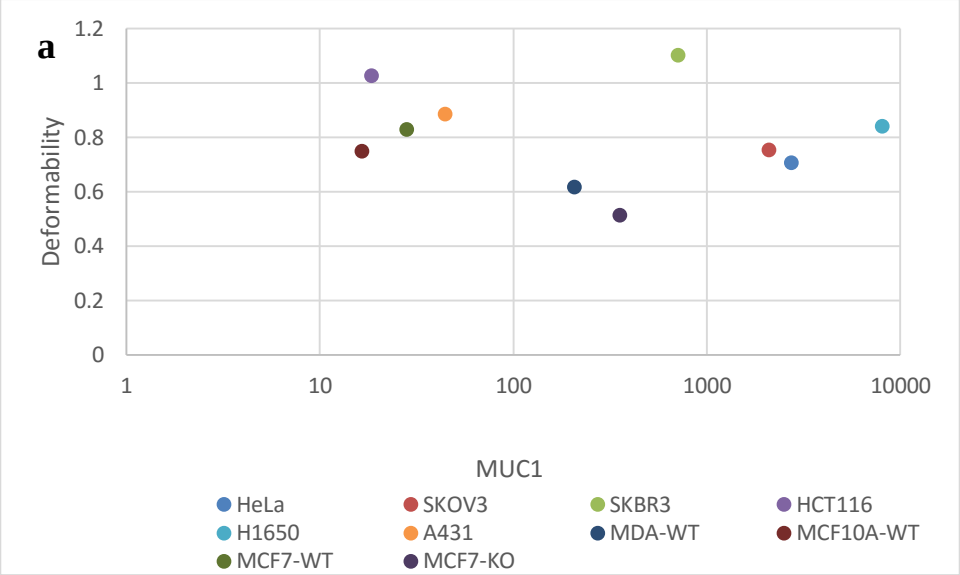

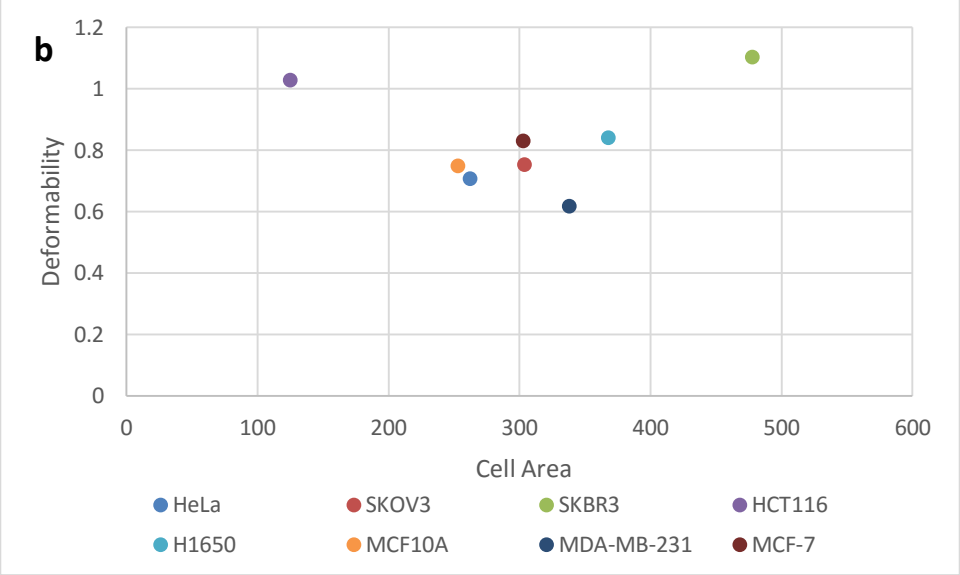

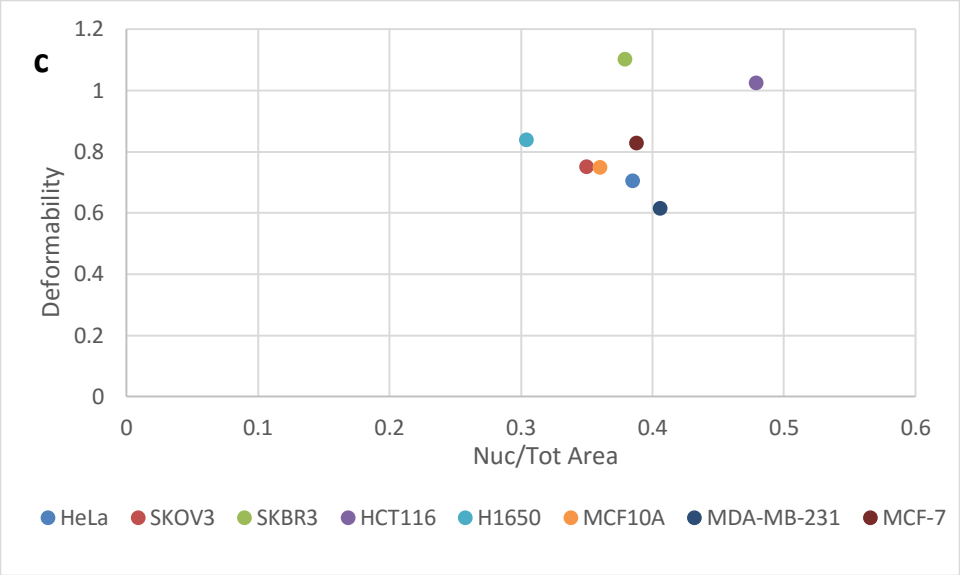

Figure 27- (a) Deformability Vs. MUC1 expression detected with Fitzgerald antibody for, (b) Deformability Vs. cell size, (c) Deformability Vs. ratio of the nucleus to total area for all the studied cell lines

Preliminary results show that in addition to the observable pattern between Mucin-1 expression and deformability values of the cells, we can see an increasing trend in deformability with increased cell size and inverse trend between the deformability and high nucleus to total size ratio, with few outlier exceptions. In the future we will investigate more on the dominant factors for each force to understand how and to what extent they contribute to these recognized trends.

References

[1] *"What Is Cancer?"*, National Cancer Institute, 9 Feb. 2015. Web. 1 May. 2016

[2] *"Cancer Diagnosis"*, National Cancer Institute, 9 Mar. 2015. Web. 1 May. 2016.

[3] *"Tumor Markers"* National Cancer Institute, 4 Nov. 2015. Web. 1 May. 2016.

[4] *"Cancer Treatment: Surgery",* National Cancer Institute, 29 Apr. 2015. Web. 1 May. 2016.

[5] *"Radiation Therapy"* National Cancer Institute, 29 Apr. 2016. Web. 1 May. 2016.

[6] *"Chemotherapy"* National Cancer Institute, 29 Apr. 2016. Web. 1 May. 2016.

[7] Elizabeth Mendes, *"Personalized Medicine: Redefining Cancer and Its Treatment"* American Cancer Society, 3 Apr. 2015. Web. 1 May. 2016.

[8] *"Basics of Personalized Medicine"* Personalized Medicine Project, Weebly. n.d. Web. 1 May. 2016

[9] *"The Future of Cancer Treatment: Personalized Medicine"* Herbert Irving Comprehensive Cancer Center, 3 Feb. 2014. Web. 1 May. 2016.

[10] *"Personalized Cancer Therapy" MD Anderson Cancer Center. n.d., n.p. Web. 1 May. 2016.*

[11] Whitesides, George M. *"The origins and the future of microfluidics" Nature*442.7101 (2006): 368-373.

[12] Seigneuric, R., et al. "From nanotechnology to nanomedicine: applications to cancer research." *Current Molecular Medicine* 10.7 (2010): 640-652.

[13] Saeed, Omer Osman, Rui Li, and Yulin Deng. "Microfluidic approaches for cancer cell separation: Review." *Journal of Biomedical Science and Engineering* 7.12 (2014): 1005.

[14] Zhang, Zhuo, and Sunitha Nagrath. "Microfluidics and cancer: are we there yet?" *Biomedical microdevices* 15.4 (2013): 595-609.

[15] Hollingsworth, Michael A., and Benjamin J. Swanson. "Mucins in cancer: protection and control of the cell surface." *Nature Reviews Cancer* 4.1 (2004): 45-60.

[16] Ryan Robinson, Stefan Pellenz, *"What is flow cytometry (FACS analysis)?",* antibodies-online. 12 June. 2013. Web. 1 May. 2016.

[17] *"Mucin 1 Antibody (VU4H5): sc-7313"*, Santa Cruz Biotechnology Inc., n.d. Web. 1 May. 2016.

[18] Rowat, Amy C., et al. "Towards an integrated understanding of the structure and mechanics of the cell nucleus." *Bioessays* 30.3 (2008): 226-236.

[19] Gossett, Daniel R., et al. "Hydrodynamic stretching of single cells for large population mechanical phenotyping." *Proceedings of the National Academy of Sciences* 109.20 (2012): 7630-7635.

[20] Dudani, Jaideep S., et al. "Pinched-flow hydrodynamic stretching of single-cells." *Lab on a Chip* 13.18 (2013): 3728-3734.

[21] *"Laminar Flow"* Wikipedia. 28 Apr. 2016. Web. 1. May. 2016

[22] Di Carlo, Dino, et al. "Continuous inertial focusing, ordering, and separation of particles in microchannels." *Proceedings of the National Academy of Sciences* 104.48 (2007): 18892-18897.

[23] Martel, Joseph M., and Mehmet Toner. "Inertial focusing in microfluidics."*Annual review of biomedical engineering* 16 (2014): 371.

Appendix A

Cell Culture Procedure

1. Observe the desired cell line under microscope to make sure that it has reached 70% confluency.
2. Place Trypsin, cell media, and HBSS in the water bath at 37°C for 15 minutes.
3. Aspirate the old media from the flask which contains the cells in a sterile culture hood.
4. Wash the cells with 5ml of HBSS.
5. Add 3 ml of Trypsin to cells and place the flask in 37°C, 5% CO_2 incubator for few minutes until the cells detach from the bottom of flask. The time required depends on the cell line.
6. Once the cells are detached and floating, add 7ml of the cell media to the flask to deactivate the Trypsin. Pipette up and down for 5 minutes.
7. Transfer the 10ml of the cell solution to a 15ml conical tube. Centrifuge for 3 minutes at 1.5X rpm.
8. Once complete, cell pellet could be observed on the bottom of the conical tube. Aspirate the media and trypsin solution without touching the cells.
9. After aspiration, add 5 ml of the cell media to the conical tube to break down the pellet. Pipette up and down until a homogenous mixture is obtained.
10. Take 1ml of the cell solution and add to a new flask with 14ml of fresh media.
11. Place the new flask in the incubator.

Appendix B

Photolithography Procedure

1. Blow the wafer surface with air to remove particles and clean the surface.
2. Pour negative photoresist (SU-8) on the wafer and spin coat it at 2000 rpm for 40 seconds.
3. Soft bake the wafer at 65°C for 5 minutes.
4. Hard bake the wafer at 95°C for 25 minutes.
5. Place the photo mask on the wafer and cover it with another glass slide, UV expose it for 18 seconds.
6. Bake the wafer again to stabilize the features on the wafer at 65°C for 3 minutes followed by 95°C for 7 minutes.
7. Pour developer in a cup and place the wafer there, shake well for 4 minutes and then let the wafer stay in there for another 2 minutes.
8. Rinse the wafer with more developer and ethyl alcohol and dry it off with air gun.
9. The silicon wafer is then baked for another 2 hours at 120°C to remove any moisture and to ensure that SU-8 adheres to the wafer firmly. The wafer is salinized then to makes sure that the mold does not stick to the wafer and also prevents the feature from getting off the wafer when a mold is removed. Salinization procedure is as follows:
10. Place the wafer in desiccator.
11. Pour 10 µl of 2-Mehoxysilane in a small container and place it in the same desiccator.
12. Vacuum the desiccator overnight.

13. Remove the wafer and place it in room temperature for 1 hour.